

Supplementary Information – Observation of Strong Coupling between One Atom and a Monolithic Microresonator

Takao Aoki^a, Barak Dayan, E. Wilcut, W. P. Bowen^b, A. S. Parkins^c, and H. J. Kimble

Norman Bridge Laboratory of Physics 12-33, California Institute of Technology, Pasadena, California 91125, USA

T. J. Kippenberg^d and K. J. Vahala

T. J. Watson Laboratory of Applied Physics, California Institute of Technology, Pasadena, California 91125, USA

(Dated: August 29, 2006)

Supporting documentation of the experimental procedures and theoretical model is provided for our manuscript Ref. [1].

I. EXPERIMENTAL DETAILS

Preparation and characterization of cold atoms – Each measurement cycle in our experiment takes about 2.5 sec, and includes approximately 2 seconds for loading a magneto-optical trap (MOT), followed by 20 ms of polarization-gradient cooling of the atoms (with the magnetic fields for the MOT turned off). The trapping and cooling beams are then switched off and the atoms fall on the microtoroid.

For each run, we measure the number and arrival times of atoms in the falling atom cloud 2 mm above the microtoroid with a laser beam resonant with the $6S_{1/2}, F = 4 \rightarrow 6P_{3/2}, F' = 4'$ transition [2]. In each cycle we observe approximately 30 atom transits during the center 10 ms of our data-collection time window. This value is in a reasonable agreement with the theoretically calculated rate of 20 transits, which was derived by comparing the measured density of the falling atom cloud to the numerically calculated interaction area of the evanescent field. Every cycle with cold atoms is followed by an identical cycle with no trapped atoms for which the magnetic field for the MOT is turned off during the loading period. We also carried out other tests for the “no atoms” case, including switching off the repumping light for the MOT (with all other parameters unchanged).

Excitation and detection system – The frequency ω_p of the probe beam P_{in} in Fig. 1(a) of the main text is actively stabilized to a fixed detuning from the atomic resonance $\Delta_A = \omega_A - \omega_p$ via saturation spectroscopy to within ± 100 kHz. The cavity resonance at ω_C is monitored relative to ω_A and ω_p for each drop of the atom cloud and each reference cycle, and is controlled by temperature-tuning a thermoelectric device upon which the Silicon chip is mounted, with a frequency shift of approximately 3 MHz per mK of temperature change. Data is automatically recorded whenever the condition of critical coupling (i.e. $P_F < 1\%$ of the maximal value of 30 counts per $2\mu\text{s}$) was achieved, corresponding to $\omega_p = \omega_C$ to within ± 2 MHz. Note that in our experiment we use blue detuning of the cavity and the probe relative to the atom, since red detuning could lead to a resonant interaction with the $6S_{1/2} F=4 \rightarrow 6P_{3/2} F' = 4'$ transition at large atom-cavity detuning $\Delta_{AC} \equiv \omega_C - \omega_A$. Additionally, blue detuning leads to an under-estimation of g , as the dipole forces become increasingly repulsive as we blue-detune our cavity, possibly leading to a more rapid reduction in the probability of transits. However, our calculations indicate that in our current experimental settings the light forces are significantly smaller than the van der Waals forces over the entire relevant interaction region of the atom with the evanescent field, and their effect on the atom’s motion and temperature is small. This situation is mostly due to the small populations of the dressed states that are coupled to the atom for excitation with $\omega_p \approx \omega_C$. Specifically, in our experiment the probe field frequency is always tuned to the empty cavity resonance, between the two vacuum-Rabi sidebands which correspond to the two dressed states of the atom and the coupled cavity mode (as described in Fig. 1). Thus, as the energy splitting between these states (and hence the associated dipole potential) grows during the atom transit, their population drops dramatically (and so does their contribution to the mechanical potential experienced by the atom), as they decouple from the probe field, leading to the described increase in the forward flux T_F . The resulting forces are of the order of few MHz/ μm , leading to estimated displacements of up to 40 nm during the $2\mu\text{s}$ of atom transit for intermediate values of Δ_{AC} . Further measurements to explore the effect of light forces along with its inclusion in the theoretical model are in progress.

The probe P_{in} enters the vacuum apparatus by way of a single-mode fiber through a Teflon feedthrough [3]. This fiber is spliced to the fiber taper. The forward propagating signal P_F in Fig. 1(a) of the main text exits the vacuum chamber in the same fashion. P_F is then directed to a 50:50 fiber beam splitter whose outputs are detected by a pair of single-photon counting modules (SPCMs) (D_{F1}, D_{F2}) each with overall quantum efficiency $\alpha \simeq 0.5$ and dark counts < 100 per second. Using two detectors enables us to avoid, or at least assess, phenomena that are related to the non-ideality of these detectors, such as their ~ 50 ns dead time, saturation at fluxes exceeding a few million counts per

second, “after-pulsing” effects which may result in a false second count, etc. Thus, two detectors allow the detection of photons that are separated temporally by less than the dead time of these detectors (which are not number-resolving), and increases the maximal flux of photons that can be detected by our system before saturation effects take place. This method also enables further analysis of the photon statistics of the light, such as the cross-correlation between the two series of photon counts presented in Fig. 3(c) of the main text.

Detection events from (D_{F1}, D_{F2}) are time-stamped relative to the drop time of the atom cloud, and stored for later analysis. The data in the figures refers to the total counts from the combined outputs of (D_{F1}, D_{F2}) . The overall propagation efficiency ξ from the fiber taper at the position of the toroidal resonator to the input beam splitter for (D_{F1}, D_{F2}) is $\xi = 0.70 \pm 0.02$. An additional SPCM was used to monitor the backwards flux, namely light that was coupled into the cavity, scattered into the counter-propagating mode and then transmitted backwards into the taper. When atom transits occurred, the observed increase in the forward flux was accompanied by a decrease in this backward flux.

In the absence of an atom, the average intracavity photon number is $\bar{n}_0 \simeq 0.3$ for the forward propagating mode (a) for critical coupling at $\omega_p = \omega_C$. If the probe is then detuned such that $|\omega_p - \omega_C| \gg \kappa$, the average number of counts recorded in a $2 \mu\text{s}$ interval is $C_{\Delta \gg \kappa} \approx 30$, which provides a calibration of the flux P_F given the known propagation and detection losses.

II. THEORY FOR A TWO-LEVEL ATOM COUPLED TO TWO TOROIDAL MODES

To understand our observations in quantitative terms, we have developed a theoretical model for a two-level atom interacting with the quantized fields of the toroidal resonator. The two-level atom has transition frequency ω_A and raising and lowering operators σ^\pm . The two counter-propagating modes of the toroidal resonator are taken to be degenerate with common frequency ω_C (in the absence of scattering), and are described by annihilation (creation) operators a (a^\dagger) and b (b^\dagger), respectively. In our actual resonators, modes are coupled due to scattering with a strength that is parameterized by h . A coherent probe of frequency ω_p in the input field of the fiber taper, a_{in} , couples to mode a with a strength \mathcal{E}_p . The input field to mode b is taken to be vacuum as in our experiments. In a frame rotating at the probe frequency ω_p , a simple Hamiltonian that models our system is thus [4]

$$\begin{aligned} H/\hbar = & \Delta_A \sigma^+ \sigma^- + \Delta (a^\dagger a + b^\dagger b) + h (a^\dagger b + b^\dagger a) \\ & + (g_{\text{tw}}^* a^\dagger \sigma^- + g_{\text{tw}} \sigma^+ a) + (g_{\text{tw}} b^\dagger \sigma^- + g_{\text{tw}}^* \sigma^+ b) \\ & + (\mathcal{E}_p^* a + \mathcal{E}_p a^\dagger), \end{aligned} \quad (1)$$

where $\Delta_A = \omega_A - \omega_p$, $\Delta = \omega_C - \omega_p$. The coherent interaction of the atom with the evanescent traveling-wave fields of the a, b modes is described by $g_{\text{tw}} = g_0^{\text{tw}} \phi_{\text{tw}}^\pm(\rho, x, z)$, where the mode functions $\phi_{\text{tw}}^\pm(\rho, x, z) = f(\rho, z) e^{\pm i k x}$ with $f(\rho, z) \sim e^{-\alpha \rho}$ ($\alpha \sim 1/\lambda$). The coordinates (ρ, x, z) are derived from cylindrical coordinates (r, θ, z) , where r is the radial distance from the axis of symmetry of the toroid, with then $\rho = r - D/2$; θ is the azimuthal angle in a plane perpendicular to the symmetry axis, with $x = r\theta$ as the position around the circumference of the toroid; and z is the vertical dimension along the symmetry axis. k is the vacuum wave vector. The field decay rate for the resonator modes is $\kappa = \kappa_i + \kappa_{\text{ex}}$, where κ_i represents intrinsic losses and κ_{ex} describes extrinsic loss due to (adjustable) coupling of the modes to the fiber taper [5–7]. The atomic excited state population decays with rate 2γ .

The output field in the forward direction is given by $a_{\text{out}} = a_{\text{in}} + \sqrt{2\kappa_{\text{ex}}} a$ [8]. Assuming only weak excitation of the atom, we can compute the output photon flux from this relationship and a linearized approximation to the equations of motion for the atomic coherence $\langle \sigma^- \rangle$ and field amplitudes $\langle a \rangle$ and $\langle b \rangle$. Characteristic spectra $T_F(\omega_p)$ of the forward flux P_F as a function of probe detuning and for different x -coordinates of the atom are shown in Fig. 1, where $|g_{\text{tw}}|/2\pi = 70/\sqrt{2}$ MHz and $\Delta_{AC} = 0$. The spectra are normalized by the flux of a far-off-resonant probe field. Also shown is the spectrum in the absence of an atom ($g_{\text{tw}} = 0$), under the (experimental) conditions of critical coupling; specifically, where $\kappa_{\text{ex}} = \kappa_{\text{ex}}^{\text{cr}} = \sqrt{\kappa_i^2 + \hbar^2}$, for which $P_F(\Delta = 0) \approx 0$ [5–7].

The coupled-atom spectra shown in Fig. 1 can be understood by considering the normal modes of the microtoroidal resonator, $A = (a + b)/\sqrt{2}$ and $B = (a - b)/\sqrt{2}$, in terms of which the Hamiltonian can be written

$$\begin{aligned} H = & \Delta_A \sigma^+ \sigma^- + (\Delta + h) A^\dagger A + (\Delta - h) B^\dagger B \\ & + \frac{1}{\sqrt{2}} [\mathcal{E}_p^* (A + B) + \mathcal{E}_p (A^\dagger + B^\dagger)] \\ & + g_A (A^\dagger \sigma^- + \sigma^+ A) \\ & - i g_B (B^\dagger \sigma^- - \sigma^+ B). \end{aligned} \quad (2)$$

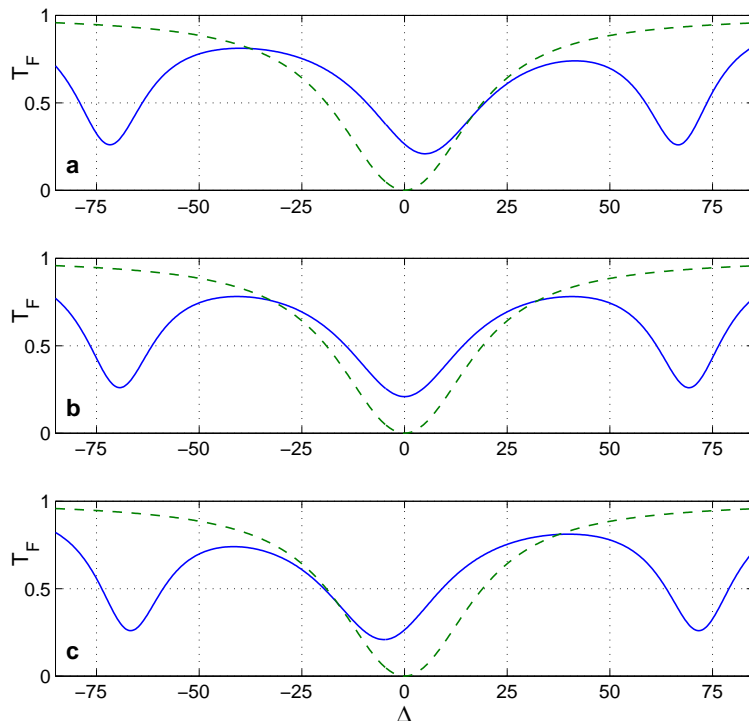


FIG. 1: Calculated spectra T_F of the forward flux in the presence of an atom (solid blue line) as a function of probe detuning Δ for different x -coordinates around the circumference of the toroid, namely (a) $kx = 0$, (b) $kx = \pi/4$, (c) $kx = \pi/2$. In all cases, $\Delta_{AC} = 0$ and $g_0/2\pi = 70$ MHz as appropriate for an atom at the external surface of our toroid. Also shown as the dashed curve is the spectrum in the absence of an atom ($g_0 = 0$) under the same conditions of critical coupling. $T_F(\omega_p)$ is normalized by the probe flux far off resonance, with (κ, h) determined from fits as in Fig. 2 in the main text.

The coherent coupling for the (A, B) modes is given here by $g_{A,B} = g_0 \psi_{A,B}(\rho, x, z)$, where $g_0 = \sqrt{2}g_0^{\text{tw}}$. The mode functions $\psi_{A,B}(\rho, x, z)$ for the normal modes of the cavity are $\psi_A(\rho, x, z) = f(\rho, z) \cos(kx)$ and $\psi_B(\rho, x, z) = f(\rho, z) \sin(kx)$. Significantly, the underlying description of the interaction of an atom with the toroidal resonator is thus in terms of standing waves $\psi_{A,B}(\rho, x, z)$ along the surface of the toroid. The splitting for the normal modes (A, B) induced by scattering h is displayed for undercoupling to our resonator in Fig. 2 of the main text.

With reference to Fig. 1(a,c), we see that for $kx = 0$ ($\pi/2$) the atom couples only to mode A (B) of frequency $\omega_C + h$ ($\omega_C - h$) with strength g_0 , leading to a pronounced reduction in T_F at probe detunings $\Delta \simeq -h \pm g_0$ ($h \pm g_0$) for the case $\Delta_{AC} = 0$ shown, i.e., at the “vacuum-Rabi sidebands”. The central feature in the transmission spectrum T_F at $\Delta = h$ ($-h$) is the spectrum of the uncoupled normal mode B (A). By contrast, at $kx = \pi/4$ in (b), the atom couples with equal strength to both normal modes and a system of three coupled oscillators is realized (in the linear approximation), the normal mode frequencies of which occur at ω_C and $\sim (\omega_C \pm g_0)$ for $\Delta_{AC} = 0$.

The eigenvalues of the atom-toroid coupled system are drawn in Fig. 2(A) relative to the cavity resonance (blue, dashed), using the same parameters as Fig 1(b). In this representation the atom (red, dashed) has positive energy detuning for negative values of Δ_{AC} , and negative detuning for positive values of Δ_{AC} . The coupling with the atom lifts the degeneracy between the atom and the cavity at Δ_{AC} , leading to the expected splitting of $2g$ between dressed states #1 and #2. However, since the atom is never fully coupled to both normal modes (A, B) , a third dressed state (#3, green) remains practically unchanged by the atom. This three mode structure is represented in both Fig. 1(a-c) and Fig. 2(B), which illustrate the transmission T_F at fixed $\Delta_{AC} = 0$ as a function of the probe frequency, demonstrating minima at 0 and $\pm g$. Similarly, the coupling strength manifests itself in the dependence of T_F on Δ_{AC} , as shown in Fig 2(C) for probe frequency fixed to the cavity resonance, as is the case in our experiment. Thus, the decrease in the forward flux T_F at the cavity resonance $\omega_p = \omega_C$ as a function of the cavity-atom detuning Δ_{AC} is a generic feature of the eigenvalue structure of the system.

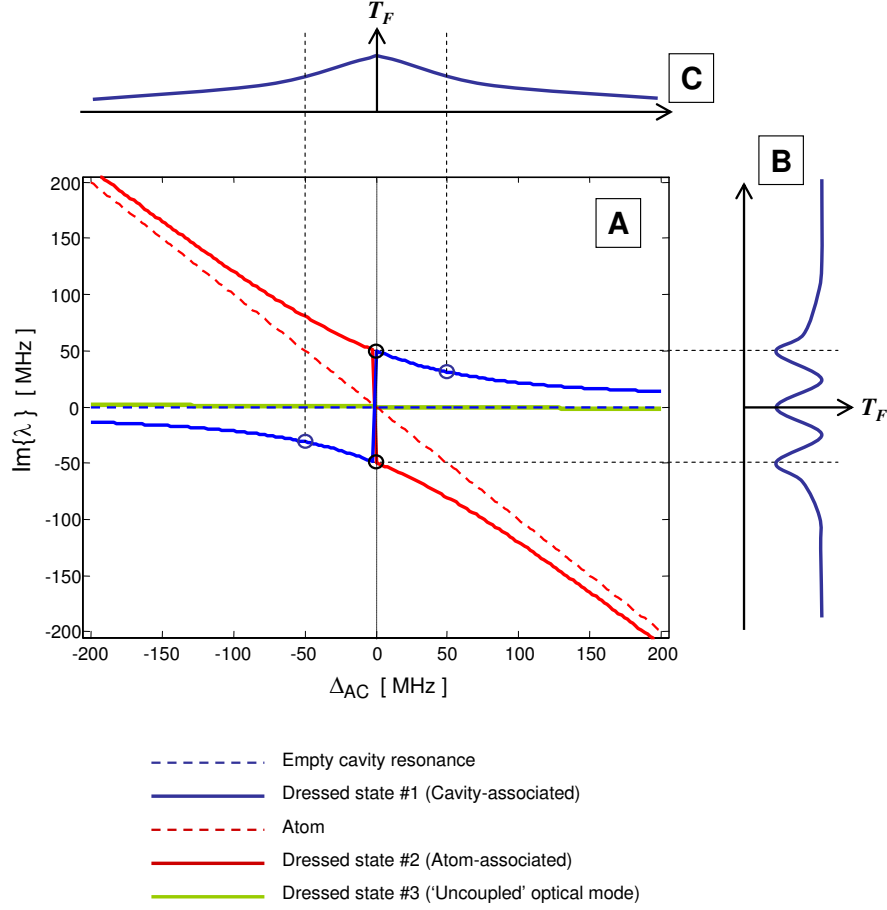


FIG. 2: (A) The three calculated eigenvalues of atom-toroid coupled system for $(g, \kappa, h) = (50, 18, 5)$ MHz. (B,C) Qualitative illustrations of the transmission T_F , (B) at fixed atom-cavity detuning $\Delta_{AC} = 0$ as a function of the probe frequency ω_p , and (C) as a function of Δ_{AC} , with probe frequency fixed to be $\omega_p = \omega_C$.

Explicitly, under conditions of critical coupling, T_F can be expressed as

$$T_F|_{\omega_p = \omega_C} = \frac{4\kappa_i^2 |g_{tw}|^4 + h^2 (g_{tw}^2 + (g_{tw}^*)^2)^2}{\left[(\gamma/2) (h^2 + \kappa^2) + 2\kappa |g_{tw}|^2 \right]^2 + [\Delta_{AC} (h^2 + \kappa^2) - h (g_{tw}^2 + (g_{tw}^*)^2)]^2}. \quad (3)$$

This is simply a Lorentzian centered at

$$\Delta_{AC}^{center} = \frac{h}{h^2 + \kappa^2} (g_{tw}^2 + (g_{tw}^*)^2), \quad (4)$$

(note that when averaged over the azimuthal coordinate x , Δ_{AC}^{center} approaches zero), and with half-width

$$\beta = \frac{\gamma}{2} + \frac{2\kappa |g_{tw}|^2 + h (g_{tw}^2 + (g_{tw}^*)^2)}{h^2 + \kappa^2} \simeq \frac{2|g_{tw}|^2}{\kappa} = \frac{|g_0|^2}{\kappa}, \quad (5)$$

assuming $2|g_{tw}|^2/\kappa \gg \gamma/2$ and $h/\kappa \ll 1$. The above result for T_F , averaged over the azimuthal coordinate x , is shown in Fig. 3 as a function of Δ_{AC} and $g_0 = \sqrt{2} g_{tw}$. Note that the half-widths of the curves $T_F(\Delta_{AC})$ are well-approximated by g_0^2/κ . Radial and temporal averaging leads to substantial narrowing of the curves $T_F(\Delta_{AC})$, producing a $\beta_{\text{effective}}$ which, while significantly smaller than the β defined in Eq. (5), maintains the dependence on the maximum coupling strength g_0^m , as illustrated in Fig. 4 of the main text. Therefore, given knowledge of κ and γ , a measurement of the

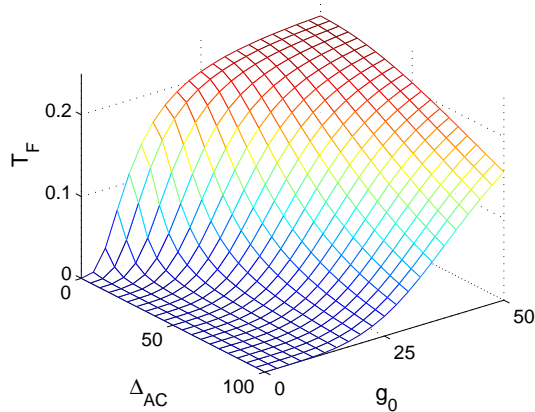


FIG. 3: Theoretical calculation for transmission $T_F(\omega_p = \omega_C)$ as a function of (Δ_{AC}, g_0) , with (κ_i, h) determined from fits to experimental data.

dependence of T_F on Δ_{AC} yields g_0 directly.

Note that the linear model presented here is adequate for the regime of our current experiment, as we have confirmed by numerical solutions of the full master equation. For the probe resonant with the cavity frequency, $\omega_p = \omega_C$, the population in the atomic excited state remains negligible for the conditions of our experiment.

It is interesting to contrast our model and the conventional Jaynes-Cummings model, which considers a two-level system coupled to only one electromagnetic field mode (for a given polarization), as is typically the case with Fabry-Perot resonators. As described above, unlike the two dressed states of the Jaynes-Cummings model, there are three eigenstates in our case. In the specific cases of $kx = 0, \pi/2$, two dressed states correspond to the vacuum-Rabi sidebands resulting from the coupling of the atom to one normal mode, while the third is essentially the normal mode that remains uncoupled with the atom. In principle, given that the coupling to the atom is stronger than the intermode coupling h , the definition of the normal modes could be chosen so the atom is at the node of one, and at the anti-node of the other for every value of kx . Thus, unlike the situation with Fabry-Perot resonators, where the atom could experience strong coupling at the anti-nodes of the standing wave and remain uncoupled to the cavity at the nodes of the standing wave, here the atom always obtains roughly the same degree of coupling with the cavity (either through one mode, the other or both). Accordingly, roughly half of the light in the cavity always remains uncoupled to the atom, leading to the third eigenvalue around zero detuning, as described in Fig 1. Note also that the presence of the atom redistributes the intensity between the two normal modes [9]. Finally, the existence of two normal modes leads to the factor of $\sqrt{2}$ between the coupling constant in our case and the one predicted by the Jaynes-Cummings model for a traveling wave $g_0 = \sqrt{2}g_0^{tw}$. Note that for the single-mode Jaynes-Cummings model, Eq. (3) takes the form

$$T_F = \frac{\left(|g_{tw}|^2 / \kappa\right)^2}{\left(\gamma/2 + |g_{tw}|^2 / \kappa\right)^2 + \Delta_{AC}^2}, \quad (6)$$

illustrating the same Lorentzian dependence on Δ_{AC} , with half-width $\beta_{JC} \sim |g_{tw}|^2 / \kappa$ for $|g_{tw}|^2 / \kappa \gg \gamma/2$.

III. CALCULATION OF THE COHERENT COUPLING PARAMETER g_0

For our particular toroidal resonator with major diameter $D \simeq 44 \mu\text{m}$ and minor diameter $d \simeq 6 \mu\text{m}$, we find numerically the lowest order traveling-wave mode functions $\phi_{tw}^\pm(\rho, x, z)$ of the resonator [10], from which follows the coupling parameters g_0^{tw} and g_0 . For the $6S_{1/2}, F = 4, m_F = 4 \rightarrow 6P_{3/2}, F' = 5', m_{F'} = 5'$ transition of the D_2 line of atomic Cesium, we find $g_0^{tw}/2\pi = 80 \text{ MHz}$ and thus $g_0/2\pi = \sqrt{2} \times 80 \text{ MHz}$. However, a circularly polarized field is required for coupling to this transition while the toroidal resonator supports linear polarization. Hence, for atoms uniformly distributed over the set of Zeeman states $\{m_F\}$ in the $F = 4$ ground state, we calculate g_0 from an average over Clebsch-Gordan coefficients for $\Delta m_F = 0$ transitions for $6S_{1/2}, F = 4 \leftrightarrow 6P_{3/2}, F' = 5'$, leading to $g_0/2\pi = 70 \text{ MHz}$, which is the value utilized in Fig. 1 above and quoted in the main text.

Current addresses –^a TA – Department of Applied Physics, The University of Tokyo, Tokyo, Japan^b WPB – Physics Department, University of Otago, Dunedin, New Zealand^c ASP – Department of Physics, University of Auckland, Auckland, New Zealand^d TJK – Max Planck Institute of Quantum Optics, Garching, Germany

-
- [1] Takao Aoki, Barak Dayan, E. Wilcut, W. P. Bowen, A. S. Parkins, T. J. Kippenberg, K. J. Vahala, and H. J. Kimble, “Observation of strong coupling between one atom and a monolithic microresonator” *Nature* (2006).
- [2] Ying-Cheng Chen, Yean-An Liao, Long Hsu, and Itz A. Yu, “Simple technique for directly and accurately measuring the number of atoms in a magneto-optical trap” *Phys. Rev. A* **64**, 031401(R) (2001).
- [3] E. R. I. Abraham and E. A. Cornell, “Teflon feedthrough for coupling optical fibers into ultrahigh vacuum systems” *Appl. Opt.* **37**, 1762-1763 (1998).
- [4] M. Rosenblit, P. Horak, S. Hellsby, and R. Folman, “Single-atom detection using whispering-gallery modes of microdisk resonators” *Phys. Rev. A* **70**, 053808 (2004).
- [5] M. L. Gorodetsky, A. D. Pryamikov, and V. S. Ilchenko, “Rayleigh scattering in high-Q microspheres” *J. Opt. Soc. Am. B* **17**, 1051-1057 (2000).
- [6] S. M. Spillane, T. J. Kippenberg, O. J. Painter, and K. J. Vahala, “Ideality in a fiber-taper-coupled microresonator system for application to cavity quantum electrodynamics” *Phys. Rev. Lett.* **91**, 043902 (2003).
- [7] T. J. Kippenberg, S. M. Spillane, and K. J. Vahala, “Modal coupling in traveling-wave resonators” *Opt. Lett.* **27**, 1669-1671 (2002).
- [8] C. W. Gardiner and M. J. Collett, “Input and output in damped quantum systems: Quantum stochastic differential equations and the master equation” *Phys. Rev. A* **31**, 3761-3774 (1985).
- [9] P. Domokos, M. Gangl, and H. Ritsch, “Single-atom detection in high-Q multimode cavities” *Opt. Comm.* **185**, 115-123 (2000).
- [10] S. M. Spillane, T. J. Kippenberg, K. J. Vahala, K. W. Goh, E. Wilcut, and H. J. Kimble, “Ultrahigh-Q toroidal microresonators for cavity quantum electrodynamics” *Phys. Rev. A* **71**, 013817 (2005).